THE JOURNAL OF PHYSICAL CHEMISTRY Letters

Letter

Cite This: J. Phys. Chem. Lett. 2018, 9, 63−69

pubs.acs.org/JPCL

Plasmon-Induced Ultrafast Hydrogen Production in Liquid Water

Lei Yan,[†] Jiyu Xu,[†] Fangwei Wang,[†] and Sheng Meng[†,‡,*]

[†]Beijing National Laboratory for Condensed Matter Physics and Institute of Physics, Chinese Academy of Sciences, Beijing 100190, China

[‡]Collaborative Innovation Centre of Quantum Matter, Beijing 100190, China

Supporting Information

ABSTRACT: Hydrogen gas production from solar water splitting provides a renewable energy cycle to address the grand global energy challenge; however, its dynamics and fundamental mechanism remain elusive. We directly explore by first-principles the ultrafast electron−nuclear quantum dynamics on the time scale of ∼100 fs during water photosplitting on a plasmonic cluster embedded in liquid water. Water molecule splitting is assisted by rapid proton transport in liquid water in a Grotthuss-like mechanism. We identify that a plasmon-induced field enhancement effect dominates water splitting, while charge transfer from gold to the antibonding orbital of a water molecule also plays an important role. "Chain-reaction" like rapid H_2 production is observed via the combination of two hydrogen atoms from different water molecules. These results provide a route toward a complete understanding of water photosplitting in the ultimate time and spatial limit.

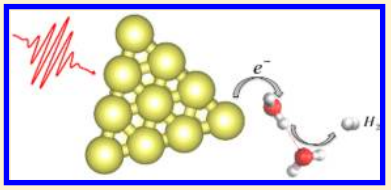

Hydrogen gas production by solar water splitting could provide a renewable energy pathway to potentially solve the world's ever-increasing energy demands.[1−3] To generate H_2, photocatalysis utilizing plasmonic excitation in supported metal structures has gained increasing attention, thanks to its dramatic light-harnessing capability and easy tunability of plasmon excitations.[4,5] Combining an oxide semiconductor with plasmonic metal nanostructures as a co-catalyst for water splitting is prevalent in the literature.[6,7] In this scenario, only hot electrons with sufficient energy to overcome the Schottky barrier can be collected by the conduction band of the semiconductor, serving as a bottleneck significantly limiting reaction efficiency. On the other hand, Robatjazi et al.[8] observed large photocurrents as a result of *direct* injection of hot electrons from plasmonic gold particles to water molecules, driving solar water splitting in a Schottky-free junction. Therefore, direct water splitting on plasmonic metal nanostructures upon photoexcitation can be achieved.[8]

Gold nanoparticles (NPs) supported on titania exhibit effective photocatalytic activity for water splitting under ultraviolet, visible, and near-infrared light.[9−11] Distinct from large particles, gold NPs show strong catalytic activities that depend on the size and shape of the supported clusters.[12−14] In general, small Au clusters maintain high stability in water solutions, making them suitable for catalytic applications.[15] A remarkable example is a Au_{20} cluster with a large electronic energy gap of 1.77 eV.[16] Its unique tetrahedral structure possesses a very high surface area and a large fraction of corner sites with low coordination,[17] which provide ideal adsorption sites to bind molecules for catalysis.

Overall, the high catalytic activity of plasmonic metal has been attributed to (i) field enhancement (FE) owing to an elevated electric field near the nanostructure[18] and (ii) electron transfer to foreign molecules by nonradiative plasmon decay.[19] It remains an open question as to which mechanism is dominant to maximize plasmon-induced photoreaction rates. Yet, a comprehensive understanding of photocatalytic water splitting, especially its femtosecond dynamics on the atomic level, has been elusive.

In this work, we investigate the atomic-scale mechanism and real-time ultrafast dynamics of water splitting and hydrogen production on model gold nanostructures irradiated by femtosecond laser pulses, based on ab initio time-dependent density functional theory (TDDFT).[20] Varying the laser intensity and frequency, we observe that the number of O−H bond splits at the end of the simulation is linearly dependent on the light intensity and compares well with the trend in optical absorption spectrum, suggesting plasmon-induced reactions. Water splitting is assisted by rapid proton transport forming hydronium ions. Analyzing localized FE in different positions, we identify that the position-dependent reaction rate has the same trend as that for the FE. In addition, we directly observe charge transfer from the gold cluster to the antibonding (AB) orbital of water from the time-evolved charge density. Overall, the plasmon-induced FE dominates the water splitting process, while the commonly assumed electron transfer plays a less important role. Most importantly, the atomic process of H_2 production via the impact of an activated hydrogen atom with another hydrogen in a water molecule in a "chain reaction" like pathway is successfully observed. These results have great implications for the complete understanding of water photosplitting and plasmon-induced photoreactions.

All calculations are performed with a real-time TDDFT code, OCTOPUS,[20] using a generalized gradient approximation in the Perdew−Burke−Ernzerhof form of the exchange−correlation functional.[21] The simulation zone is defined by assigning a

Received: November 7, 2017
Accepted: December 8, 2017
Published: December 8, 2017

DOI: 10.1021/acs.jpclett.7b02957
J. Phys. Chem. Lett. 2018, 9, 63−69

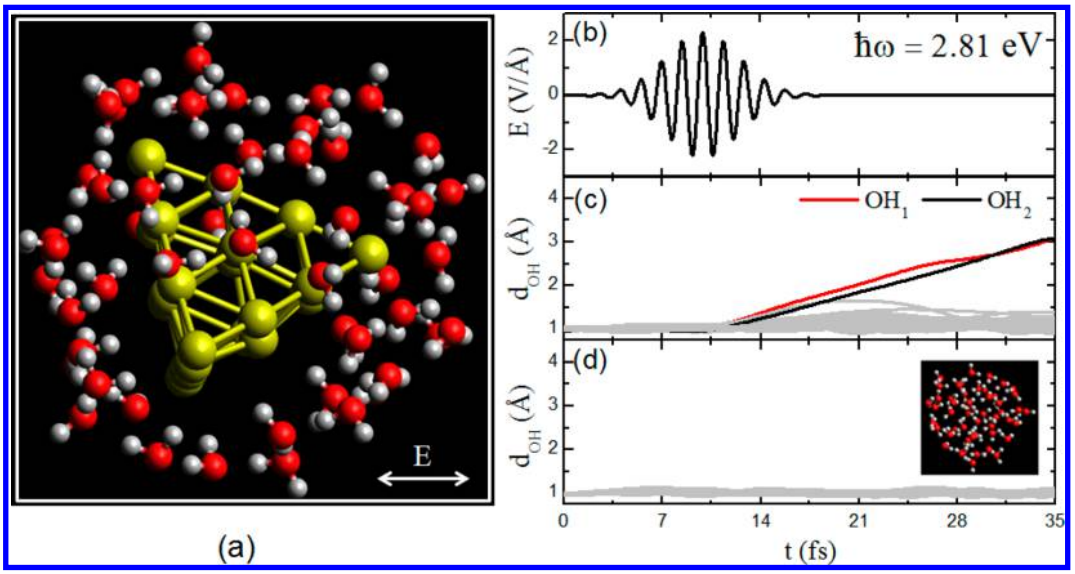

Figure 1. (a) Snapshot of the Au_{20} cluster in water, where yellow, red, and gray spheres represent gold, oxygen, and hydrogen atoms, respectively. The arrow denotes the polarization direction of the laser field. (b) Time evolution of the laser field with field strength E_{max} = 2.3 V/Å and frequency $\hbar\omega$ = 2.81 eV. Under this laser pulse, time-evolved O−H bond lengths d_{OH} of all water molecules with (c) and without (d) the Au_{20} cluster are shown.

sphere around each atom with a radius of 6.0 Å and a uniform grid of 0.25 Å. Troullier−Martins pseudopotentials[22] are used to represent the interaction between valence electrons and atomic core. To simulate the dynamics of water photosplitting, Kohn−Sham wave functions of the system under a laser field are evolved for 15 000 steps with a time step of 0.003 fs. A time propagator in the Ehrenfest scheme[23] for electron−ion dynamics is used, with an initial temperature fluctuating around 300 K.

As the Au_{20} nanocluster has a symmetric geometry and high stability,[17] we choose Au_{20} as a model NP, which is enclosed with 52 water molecules to represent a liquid water environment (see Figure 1a). The stable geometry from the ground-state molecular dynamics (MD) simulations at room temperature (300 K) is selected as the starting condition for TDDFT-MD simulations. In the initial configuration, three water molecules bond to the corner site of the Au_{20} cluster by forming Au−O bonds (bond length: 2.3 Å). These bonds enhance the Lewis base character of Au atoms that are not connected to water molecules, thereby preventing further bonding of water molecules to the Au_{20} cluster.

We first explore optical absorbance of the Au_{20}−water system (Figure 1). The adsorption spectrum shows a dominant peak at 2.81 eV (Figure S1), in good agreement with the value of 2.78 eV in the literature.[12] This peak is composed of multiple electronic excitations and is identified as plasmon resonance.[3,24] Other peaks at 1.73 and 2.30 eV are too weak in intensity to excite collective plasmon resonance. The peaks at 3.4−3.6 eV are ascribed to excitations from the vertex atoms of Au_{20} clusters.[12,24] They are in the ultraviolet range, and therefore, they are out of scope here. The liquid water environment induces a red shift of 0.05 eV for the major absorption peak. The red shift in resonant energy can be understood by spontaneous charge transfer from Au_{20} to nearby water molecules.[25]

Femtosecond laser pulses provide a powerful tool to engineer electronic excitations and to study ultrafast dynamics of chemical reactions.[26,27] To mimic a laser pulse, we apply an external field with a Gaussian envelope $E(t) = E_{max}\exp\left[-\frac{(t-t_0)^2}{2\tau^2}\right]\cos(\omega t - \omega t_0)$, as shown in Figure 1b. Due to forbidding computational costs in TDDFT quantum dynamics simulations, we utilize a strong laser field to accelerate photoreactions to make direct simulations of water photosplitting feasible. The laser field reaches the maximum amplitude E_{max} = 2.3 V/Å at the time t_0 = 10 fs, corresponding to a laser intensity of $\sim 7 \times 10^{13}$ W/cm^2 and fluence of ~0.16 J/cm^2. To observe the ultrafast process of water splitting, we use a laser intensity of $\sim 10^{13}$ W/cm^2, which is far above the average power of territorial solar irradiance. We note that few-cycle laser pulses with an intensity of $\sim 10^{13}$ W/cm^2 and fluence of ~0.1 J/cm^2 are widely available and easily applied in typical ultrafast laser experiments.[28] Considering the ultrafast photon−NP interaction time ($\sim 1 \times 10^{-9}$ m / 3×10^8 m/s $\approx 10^{-18}$ s) and a typical energy of 2.5 eV per solar photon, a field strength of 2.5 eV/10^{-18} s per area of NP $\approx 10^{13}$ W/cm^2 is also relevant for the quantum nature of photosplitting under solar irradiance. The laser frequency in the following simulations is set to the resonant energy of 2.81 eV to activate plasmon excitation in Au_{20}, unless otherwise specified. We emphasize that, although the laser field apparently seems very strong, laser pulse duration is too short (~10 fs) to induce significant local heating or structural damage in the gold cluster.

We then investigate the dynamic response of water on a Au_{20} cluster to the laser field as shown in Figure 1c, which displays the time-dependent O−H bond length d_{OH} for all water molecules around the Au_{20} cluster. In the first 10 fs, all O−H bonds oscillate with the amplitude ~0.05 Å or less. During the timespan of t = 10−30 fs, oscillation amplitudes for most O−H bonds increase by less than 0.5 Å and then gradually decrease after t = 30 fs due to attenuation of the laser pulse. However, two O−H bonds separately from two water molecules keep increasing their bond length from d_{OH1} = 1.07 Å (d_{OH2} = 0.97 Å) at t = 10 fs to 3.11 Å (3.09 Å) at t = 35 fs. That is, two water molecules split into a hydroxyl group (OH) and hydrogen atom within 35 fs. In contrast, for liquid water without the presence

DOI: 10.1021/acs.jpclett.7b02957
J. Phys. Chem. Lett. 2018, 9, 63−69

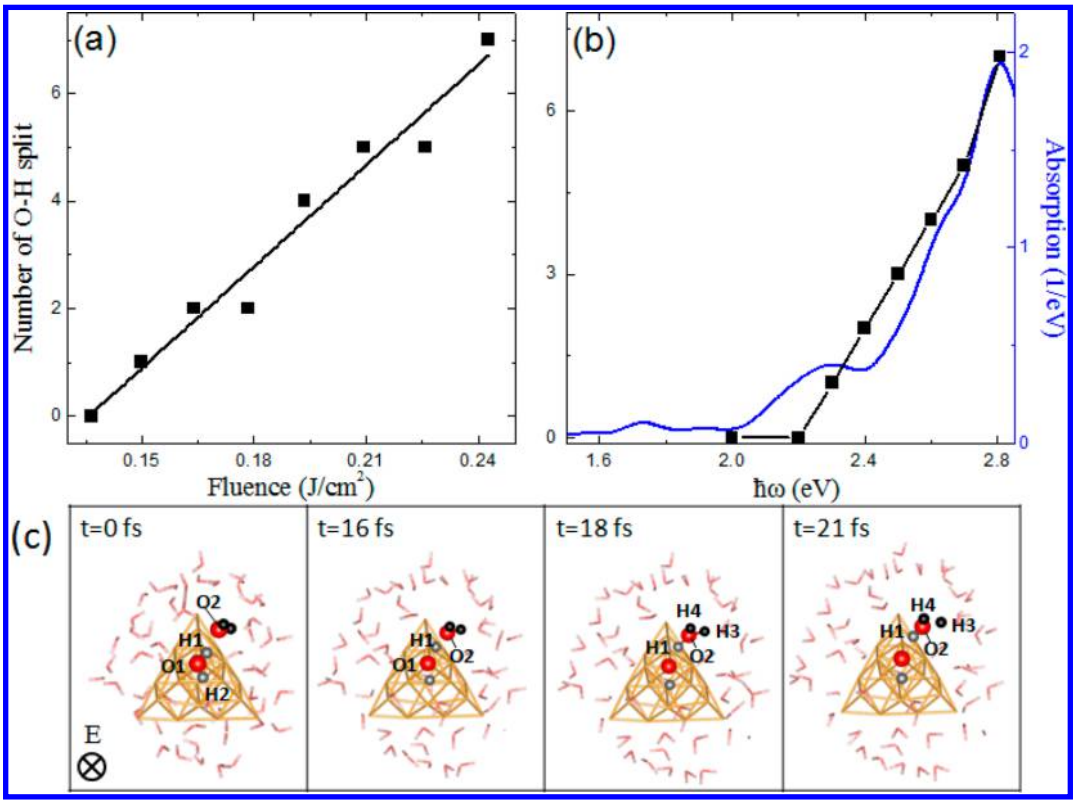

Figure 2. (a) Number of O−H bond splits with varied laser fluence, corresponding to a field strength from E_{max} = 2.1 to 2.8 V/Å. Linear fits to data points are shown as the black line. (b) Number of O−H bond splits with varied laser frequency for the fixed field strength E_{max} = 2.8 V/Å. The corresponding absorption spectrum (blue lines) is superimposed for comparison. (c) Atomic configurations at times t = 0, 16, 18, and 21 fs.

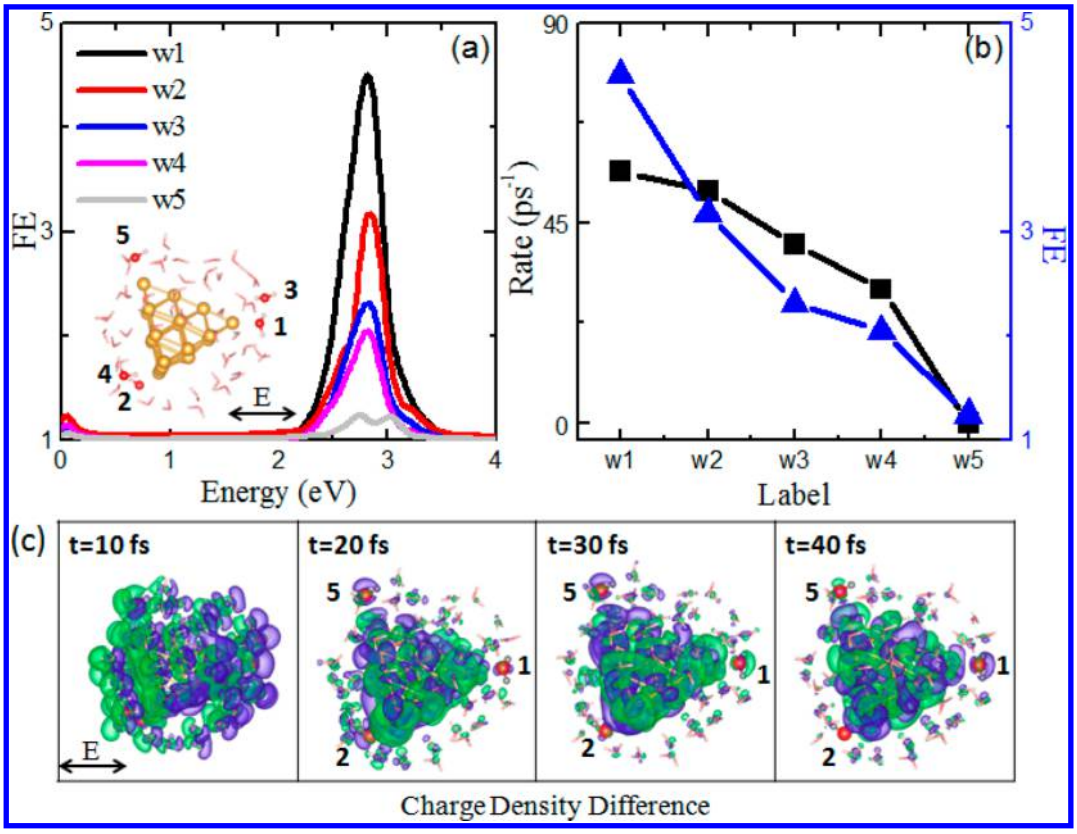

Figure 3. (a) FE along the laser polarization direction for the Au_{20} cluster as a function of laser energy in different positions as defined in the inset. (b) Position dependence of the FE (blue line) and the corresponding rate for water splitting (black line) under a laser field of E_{max} = 2.7 V/Å. (c) Charge density difference at times t = 10, 20, 30, and 40 fs.

DOI: 10.1021/acs.jpclett.7b02957
J. Phys. Chem. Lett. 2018, 9, 63−69

of a Au_{20} cluster, all of the O−H bonds oscillate continuously and never break under the same laser illumination (Figure 1d). Therefore, we confirm that water splitting is mediated by the Au_{20} cluster.

To better understand the plasmon-induced water splitting reaction, we probe the dynamic response of the system using different laser fluences, shown in Figure 2a. In the following, we deem that the O−H bond splits whenever its length reaches 2.0 Å. We find that the number of O−H splits is linearly dependent on the laser fluence, implying a single-photon process.[29] We note that the linear line in Figure 2a does not go across the origin, which is due to the fact that a critical laser fluence is needed for the observation of water splitting here.[30] In experiments, this linear relationship has been observed for hydrogen dissociation on Au NPs[30] and ethylene epoxidation on Ag nanocubes.[31] Figure 2b shows wavelength dependence for the number of split O−H bonds, which compares well with the overall shape of the optical absorption spectrum. This further confirms that water splitting is induced by plasmon excitation of Au_{20}, in good agreement with previous experiments.[32−34]

To illustrate the atomic processes during water splitting, Figure 2c shows typical snapshots of the time-dependent atomic configuration. Initially (t = 0 fs), a water molecule consisting of two hydrogens (labeled as H1, H2) and an oxygen atom (labeled as O1) is bonded at the tip of the Au_{20} cluster and forms a hydrogen bond with another water molecule with its atoms labeled as H3, H4, and O2. Atom H1 points to atom O2 with distance d_{O2-H1} = 1.72 Å. At t = 16 fs, the distance d_{O2-H1} decreases to 1.42 Å, and the O1−H1 bond length d_{O1-H1} increases from 1.00 to 1.67 Å. That is, the H1 atom covalently bonds to both O1 and O2 atoms partially. At t = 18 fs, the distance d_{O1-H1} continues to increase to 1.89 Å, indicating that the O1−H1 bond splits, and the distance d_{O2-H1} is 1.35 Å. At the same time, the distance d_{O2-H3} begins increasing to 1.31 Å and d_{O2-H4} reaches 1.27 Å. Namely, atoms O2, H1, H3, and H4 form a hydronium ion. At t = 21 fs, the distance d_{O2-H3} increases to 1.57 Å, while d_{O2-H1} decreases to 1.26 Å. Subsequently, d_{O2-H3} keeps increasing and reaches 2.0 Å at t = 26 fs (Figure S2). That is, the O2−H3 bond splits, whereas d_{O2-H4} and d_{O2-H1} oscillate around 1.0 Å and reach values of 1.06 and 1.10 Å after t = 26 fs, respectively. Therefore, water splitting is assisted by proton transfer in the Grotthuss-like mechanism, as observed in hydrogen-bonded acid−base complexes in liquid water.[35] We find that forming hydrogen bonds accelerates water splitting (see Figure S3).

To gain further insights into reaction mechanisms, we display the FE spectrum at different positions around the Au_{20} cluster in Figure 3a. These positions are adsorption sites for water molecules labeled as w1, w2, w3, w4, and w5. Here the localized FE factor is defined as $FE(x) = [v_{eff}(x + \delta x) - v_{eff}(x)]/e\delta x E_{ext}$, where x is the position, δx is the mesh size along the polarized direction, v_{eff} is effective potential, and E_{ext} is the external field strength.[36] A peak appears in the FE spectrum around a laser frequency of 2.81 eV for all cases. The peak values are 4.5, 3.2, 2.3, 2.0, and 1.2, decreasing in turn from w1 to w5, as shown in Figure 3b. Among them, w1 is located on the tip of the Au_{20} cluster, showing the largest FE. We also show the FE in a transverse cut going through the tip atom and find that the largest FE is ∼7.0 at the tip of Au_{20} (Figure S4). Similar tip-enhanced FE reaches a value of 7.1 on a larger cluster Ag_{489},[37] of the same magnitude as our result.

For simplicity, we define the rate of water splitting as the inverse of the time needed for breaking the first O−H bond, when its length reaches 2.0 Å. We find that the reaction rates for water placed at positions w1 to w5 are 56.6, 52.2, 40.1, 30.0, and 0.0 ps^{-1}, also decreasing in turn (Figure 3b). The trend of a position-dependent reaction rate closely follows that of FE. Thus, we conclude that the reaction rate for water photo-splitting on Au_{20} is dominantly determined by plasmon-induced FE.

However, the reaction rate does not follow exactly the trend in the FE. To figure it out, we illustrate the time evolution of charge density in Figure 3c. The charge density difference between that at a given time t and at t = 0 is shown. At t = 10 fs, the charge density oscillates following the external field. At t = 20 fs, when the laser field fades out, part of electrons transfer to the AB orbitals of w2 and w5, while w1 only receives a small amount of electrons on the oxygen atom. Instantaneous charge transfer also exists on a TiO_2 surface with plasmonic NPs.[38] After that, more electrons transfer from the Au_{20} cluster to the AB orbital of w1, and electrons on w2 and w5 begin to decay. However, water splitting occurs before t = 20 fs for w1 and w2, as shown in Figure 1c. Thus, we infer that w1 splits due to a large FE, and w2 splits owing to both the FE and charge transfer effect. In addition, during the simulation timespan, we have not observed the splitting of w5, though there exists clear charge transfer. The main reason is that the FE at w5 is only 1.2, implying too weak FE to split water. On the basis of the above analysis, we infer that while a plasmon-induced FE dominates, charge transfer also plays a role for water splitting on the Au_{20} cluster.

To reveal the nature of plasmon photoexcitation, we analyze the time-evolved change in the occupation of Kohn−Sham (KS) states (Figure S5a). The occupation of KS states is calculated by projecting the time-dependent KS state onto the ground-state orbitals. Before t = 20 fs, there exists oscillation for occupation near the lowest unoccupied molecular orbital (LUMO), which results from plasmon excitation.[39] After t = 20 fs, with the laser fading off, some electrons are excited from states with energy at −6.23 to −6.00 eV to the states at −3.92 to −3.42 eV with respect to the vacuum level, which is responsible for plasmon decay via Landau damping.[40]

We calculate the localized density of states (LDOS) of water molecules from w1 to w5 (Figure S5b). The AB orbitals of different water molecules appear at −3.45 eV, overlapping well with newly occupied orbitals of Au_{20} upon photoexcitation. This energy match promotes resonant charge transfer.[19] Besides, the density of the AB state in this energy range for w2 and w5 is larger than that for w1. This explains why the charge transfer in w2 and w5 is faster than that in w1. We find that the LUMO+3 orbital, which has a significant amount of p-electron character, accumulates most electrons after t = 20 fs (Figure S6a). We also calculate transition coefficients $|C_{LUMO+3,i}(t)|^2$, defined as the time-dependent occupied KS orbital $|i(t)\rangle$ projected onto the LUMO+3 state (Figure S6b). These coefficients display a gradual increase in amplitude, corresponding to hot electron generation by plasmon decay.[40] Among them, the seventh orbital below the highest occupied molecular orbital (HOMO) with d-electron character, termed HOMO−7, shows the largest transition. Thus, plasmon decay of Au_{20} is processed mainly by generating hot electrons via electronic transitions from the d-band to p-band. Similar analysis on the optical excitation of Au_{20} also reveals the importance of 5d and 6p electrons.[12]

DOI: 10.1021/acs.jpclett.7b02957
J. Phys. Chem. Lett. 2018, 9, 63−69

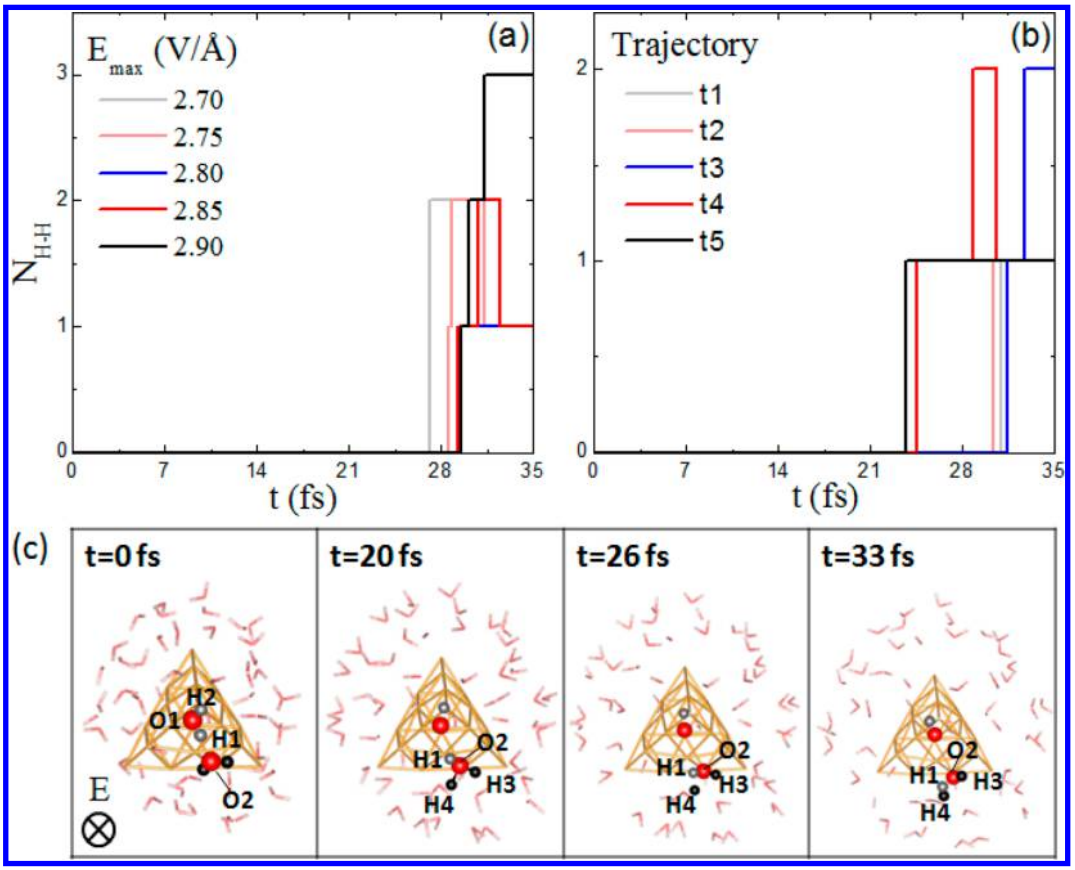

Figure 4. Time evolution of the number of hydrogen molecules (a) with varied laser intensity and (b) in separate MD trajectories with the field strength E_{max} = 2.8 V/Å. (c) Atomic configurations at times t = 0, 20, 26, and 33 fs.

More importantly, we observe rapid hydrogen production from water, as displayed in Figure 4a. We show that a hydrogen molecule is formed when its H−H bond length is less than 1.0 Å. For a laser field of E_{max} = 2.90 V/Å, three hydrogen molecules are formed gradually after 20 fs. In other cases, two hydrogen molecules are first formed, and then one of them splits. This observation is universal for different MD trajectories, where we find that a hydrogen molecule is generally produced within 35 fs, as shown in Figure 4b. Considering that the Au_{20} cluster has a size of ∼1.0 nm and the laser intensity is ∼0.2 J/cm^2 per pulse, the maximum number of photons reaching Au_{20} is ∼10000. Thus, the quantum efficiency for H_2 production is about 0.03%, similar to the reported incident-photon-to-current efficiency (0.06%) for the 2 nm thick Au NP during direct water photosplitting.[8] Without a gold cluster, however, H_2 production is unlikely to occur owing to the large energy barrier for water splitting and H recombination. Thus, the gold cluster could serve as a photocatalytic reaction center to produce H_2 from water.

The detailed process for hydrogen production is shown in Figure 4c. Initially, one water molecule with atoms labeled H1, H2, and O1 is located near the tip of the Au_{20} cluster. This molecule forms a hydrogen bond with another water molecule consisting of H3, H4, and O2 through an O2−H1 hydrogen bond with a bond length of d_{O2-H1} = 1.72 Å. At t = 20 fs, the distance d_{O2-H1} decreases to 1.55 Å, and the O1−H1 bond length d_{O1-H1} increases to 2.45 Å, indicating the split of the O1−H1 bond. Simultaneously, the H1 atom comes closer to H4 with d_{H1-H4} = 1.89 Å, and the H4 atom keeps going away from O2 with d_{O2-H4} = 1.51 Å. At t = 26 fs, the distance d_{H1-H4} decreases to 1.48 Å, and d_{O2-H4} reaches 1.91 Å, implying that the O2−H4 bond breaks up. At t = 33 fs, d_{H1-H4} reaches 0.86 Å, forming a H_2 molecule. The O2−H3 still remains bonded with a bond length of d_{O2-H3} = 0.95 Å. The details for time-evolved changes in bond length are shown in Figure S7. Therefore, a hydrogen molecule is formed via a "chain reaction" like mechanism: plasmon excitation produces intense hot electrons to activate OH bonds; an activated H then detaches from water and can be accelerated; the H from another water dissociates by the strong impact of the first H together with hot electrons, to produce a H_2 molecule.

The tip of the gold cluster is the most active site for water splitting to produce H_2. Due to plasmon-induced strong field, the activated hydrogen atom on the tip of Au_{20} would have a large momentum to take hydrogen atoms from other water molecules. Therefore, H_2 production in our simulations only occurs around the tip of the gold cluster. Indeed, the plasmon energy of the gold cluster is located well above the H_2/H_2O redox potential, high enough to overcome the barrier to produce H_2.[14] The reaction path in our simulations is similar to that of hydrogen production from water on the Al_{17} cluster in the ground-state MD simulation,[3] where the temperature is 1000 K and the time for H_2 production is ∼2 ps. Therefore, plasmon-induced water splitting to produce H_2 could be much more efficient than heat-induced reactions. Besides, OH radicals easily spread away from the Au_{20} cluster and recombine to form H_2O_2 or H_2 + O_2 on the supporting substrate (e.g., inert oxides or p-semiconductors), excluding the possibility of catalyst poisoning by reaction products.[41] Instead, an inert

DOI: 10.1021/acs.jpclett.7b02957
J. Phys. Chem. Lett. 2018, 9, 63−69

Al_2O_3 layer is formed in the case of water splitting on Al clusters.

We present the first real-time quantum simulations of water photosplitting and rapid hydrogen production on a Au_{20} cluster in water upon laser illumination. We demonstrate that plasmon-induced FE dominates the water splitting process, and charge transfer from the Au_{20} cluster to the AB state of the water molecule also contributes to photoreactions. In the experiment of photocatalytic water splitting on CdSe nanoplatelets, a 5-fold increase in photocurrent was observed after covering with Au NPs, which resulted from enhanced plasmonic fields.[42] The control of the laser parameter would then effectively tune the reaction efficiency. Gold NP-based hydrogen production from water is highly promising if the Au NPs are massively produced. These results provide fundamental insights into understanding plasmon-induced atomic processes and are helpful to improve further efficiency for solar hydrogen production.

■ ASSOCIATED CONTENT

Supporting Information

The Supporting Information is available free of charge on the ACS Publications website at DOI: 10.1021/acs.jpclett.7b02957.

Optical absorption spectrum, time evolution of bond lengths, field enhancement distribution, and population analysis of Kohn−Sham orbitals (PDF)

■ AUTHOR INFORMATION

ORCID

Lei Yan: 0000-0002-2698-4613

Sheng Meng: 0000-0002-1553-1432

Notes

The authors declare no competing financial interest.

■ ACKNOWLEDGMENTS

We acknowledge helpful discussions with S.W. Gao and financial support from MOST (Grant Nos. 2016YFA0300902 and 2015CB921001), NSFC (Grant Nos. 11774396, 11474328, and 11290164), and "Strategic Priority Research Program B" of the CAS (No. XDB070301).

■ REFERENCES

(1) Lewis, N. S. Toward Cost-Effective Solar Energy Use. *Science* **2007**, *315*, 798−801.

(2) Steinfeld, A. Solar Thermochemical Production of Hydrogen−−a Review. *Sol. Energy* **2005**, *78*, 603−615.

(3) Cushing, S. K.; Wu, N. Progress and Perspectives of Plasmon-Enhanced Solar Energy Conversion. *J. Phys. Chem. Lett.* **2016**, *7*, 666−675.

(4) Li, Y.; Zhao, K.; Sobhani, H.; Bao, K.; Nordlander, P. Geometric Dependence of the Line Width of Localized Surface Plasmon Resonances. *J. Phys. Chem. Lett.* **2013**, *4*, 1352−1357.

(5) Linic, S.; Christopher, P.; Ingram, D. B. Plasmonic-Metal Nanostructures for Efficient Conversion of Solar to Chemical Energy. *Nat. Mater.* **2011**, *10*, 911−921.

(6) Kibria, M. G.; Chowdhury, F. A.; Zhao, S.; AlOtaibi, B.; Trudeau, M. L.; Guo, H.; Mi, Z. V. Visible Light-Driven Efficient Overall Water Splitting Using p-type Metal-Nitride Nanowire Arrays. *Nat. Commun.* **2015**, *6*, 6797.

(7) Mubeen, S.; Lee, J.; Singh, N.; Kramer, S.; Stucky, G. D.; Moskovits, M. An Autonomous Photosynthetic Device in Which All Charge Carriers Derive from Surface Plasmons. *Nat. Nanotechnol.* **2013**, *8*, 247−251.

(8) Robatjazi, H.; Bahauddin, S. M.; Doiron, C.; Thomann, I. Direct Plasmon-Driven Photoelectrocatalysis. *Nano Lett.* **2015**, *15*, 6155−6161.

(9) Liu, Z.; Hou, W.; Pavaskar, P.; Aykol, M.; Cronin, S. B. Plasmon Resonant Enhancement of Photocatalytic Water Splitting Under Visible Illumination. *Nano Lett.* **2011**, *11*, 1111−1116.

(10) Nishijima, Y.; Ueno, K.; Kotake, Y.; Murakoshi, K.; Inoue, H.; Misawa, H. Near-Infrared Plasmon-Assisted Water Oxidation. *J. Phys. Chem. Lett.* **2012**, *3*, 1248−1252.

(11) Ranasingha, O.; Wang, H.; Zobač, V.; Jelínek, P.; Panapitiya, G.; Neukirch, A. J.; Prezhdo, O. V.; Lewis, J. P. Slow Relaxation of Surface Plasmon Excitations in Au_{55}: the Key to Efficient Plasmonic Heating in Au/TiO_2. *J. Phys. Chem. Lett.* **2016**, *7*, 1563−1569.

(12) Idrobo, J. C.; Walkosz, W.; Yip, S. F.; Öğüt, S.; Wang, J.; Jellinek, J. Static Polarizabilities and Optical Absorption Spectra of Gold Clusters (Au_n, n = 2−14 and 20) from First Principles. *Phys. Rev. B* **2007**, *76*, 205422.

(13) Ferrighi, L.; Hammer, B.; Madsen, G. K. H. 2D−3D Transition for Cationic and Anionic Gold Clusters: A Kinetic Energy Density Functional Study. *J. Am. Chem. Soc.* **2009**, *131*, 10605−10609.

(14) Ding, Z.; Meng, S. Promote Water Photosplitting via Tuning Quantum Well States in Supported Metal Clusters. *Phys. Rev. B: Condens. Matter Mater. Phys.* **2012**, *86*, 045455.

(15) Zheng, J.; Zhang, C.; Dickson, R. M. Highly Fluorescent, Water-Soluble, Size-Tunable Gold Quantum Dots. *Phys. Rev. Lett.* **2004**, *93*, 077402.

(16) Li, J.; Li, X.; Zhai, H. J.; Wang, L. S. Au20: A Tetrahedral Cluster. *Science* **2003**, *299*, 864−867.

(17) Zhao, L.; Jensen, L.; Schatz, G. C. Pyridine−Ag20 Cluster: A Model System for Studying Surface-Enhanced Raman Scattering. *J. Am. Chem. Soc.* **2006**, *128*, 2911−2919.

(18) Kang, J. H.; Kim, D. S.; Park, Q.-H. Local Capacitor Model for Plasmonic Electric Field Enhancement. *Phys. Rev. Lett.* **2009**, *102*, 093906.

(19) Yan, L.; Wang, F. W.; Meng, S. Quantum Mode Selectivity of Plasmon-Induced Water Splitting on Gold Nanoparticles. *ACS Nano* **2016**, *10*, 5452−5458.

(20) Andrade, X.; Strubbe, D. A.; De Giovannini, U.; Larsen, A. H.; Oliveira, M. J. T.; Alberdi-Rodriguez, J.; Varas, A.; Theophilou, I.; Helbig, N.; Verstraete, M.; et al. Real-Space Grids and the Octopus Code as Tools for the Development of New Simulation Approaches for Electronic Systems. *Phys. Chem. Chem. Phys.* **2015**, *17*, 31371−31396.

(21) Perdew, J. P.; Burke, K.; Ernzerhof, M. Generalized Gradient Approximation Made Simple. *Phys. Rev. Lett.* **1996**, *77*, 3865.

(22) Troullier, N.; Martins, J. L. Efficient Pseudopotentials for Plane-Wave Calculations. *Phys. Rev. B: Condens. Matter Mater. Phys.* **1991**, *43*, 1993.

(23) Alonso, J. L.; Andrade, X.; Echenique, P.; Falceto, F.; Prada-Gracia, D.; Rubio, A. Efficient Formalism for Large-Scale Ab Initio Molecular Dynamics Based on Time-Dependent Density Functional Theory. *Phys. Rev. Lett.* **2008**, *101*, 096403.

(24) Wu, K.; Li, J.; Lin, C. Remarkable Second-Order Optical Nonlinearity of Nano-Sized Au_{20} Cluster: a TDDFT Study. *Chem. Phys. Lett.* **2004**, *388*, 353−357.

(25) Sheldon, M. T.; van de Groep, J.; Brown, A. M.; Polman, A.; Atwater, H. A. Plasmoelectric Potentials in Metal Nanostructures. *Science* **2014**, *346*, 828−831.

(26) Lupetti, M.; Hengster, J.; Uphues, T.; Scrinzi, A. Attosecond Photoscopy of Plasmonic Excitations. *Phys. Rev. Lett.* **2014**, *113*, 113903.

(27) Brown, A. M.; Sundararaman, R.; Narang, P.; Schwartzberg, A. M.; Goddard, W. A., III; Atwater, H. A. Experimental and Ab Initio Ultrafast Carrier Dynamics in Plasmonic Nanoparticles. *Phys. Rev. Lett.* **2017**, *118*, 087401.

(28) Baltuška, A.; Udem, Th.; Uiberacker, M.; Hentschel, M.; Goulielmakis, E.; Gohle, Ch.; Holzwarth, R.; Yakovlev, V. S.; Scrinzi, A.; Hänsch, T. W.; et al. Attosecond Control of Electronic Processes by Intense Light Fields. *Nature* **2003**, *421*, 611−615.

DOI: 10.1021/acs.jpclett.7b02957
J. Phys. Chem. Lett. 2018, 9, 63−69

(29) Kale, M. J.; Avanesian, T.; Christopher, P. Direct Photocatalysis by Plasmonic Nanostructures. *ACS Catal.* **2014**, *4*, 116−128.
(30) Mukherjee, S.; Libisch, F.; Large, N.; Neumann, O.; Brown, L. V.; Cheng, J.; Lassiter, J. B.; Carter, E. A.; Nordlander, P.; Halas, N. J. Hot Electrons Do the Impossible: Plasmon-Induced Dissociation of H_2 on Au. *Nano Lett.* **2013**, *13*, 240.
(31) Christopher, P.; Xin, H.; Linic, S. Visible-Light-Enhanced Catalytic Oxidation Reactions on Plasmonic Silver Nanostructures. *Nat. Chem.* **2011**, *3*, 467−472.
(32) Ingram, D. B.; Linic, S. Water Splitting on Composite Plasmonic-Metal/Semiconductor Photoelectrodes: Evidence for Selective Plasmon-Induced Formation of Charge Carriers near the Semiconductor Surface. *J. Am. Chem. Soc.* **2011**, *133*, 5202−5205.
(33) Shi, Y.; Wang, J.; Wang, C.; Zhai, T. T.; Bao, W. J.; Xu, J. J.; Xia, X. H.; Chen, H. Y. Hot Electron of Au Nanorods Activates the Electrocatalysis of Hydrogen Evolution on MoS2 Nanosheets. *J. Am. Chem. Soc.* **2015**, *137*, 7365−7370.
(34) Christopher, P.; Xin, H.; Marimuthu, A.; Linic, S. Singular Characteristics and Unique Chemical Bond Activation Mechanisms of Photocatalytic Reactions on Plasmonic Nanostructures. *Nat. Mater.* **2012**, *11*, 1044−1050.
(35) Rini, M.; Magnes, B.; Pines, E.; Nibbering, E. T. J. Real-Time Observation of Bimodal Proton Transfer in Acid-Base Pairs in Water. *Science* **2003**, *301*, 349−352.
(36) Song, P.; Nordlander, P.; Gao, S. Quantum Mechanical Study of the Coupling of Plasmon Excitations to Atomic-Scale Electron Transport. *J. Chem. Phys.* **2011**, *134*, 074701.
(37) Negre, C. F. A.; Perassi, E. M.; Coronado, E. A.; Sánchez, C. G. Quantum Dynamical Simulations of Local Field Enhancement in Metal Nanoparticles. *J. Phys.: Condens. Matter* **2013**, *25*, 125304.
(38) Long, R.; Prezhdo, O. V. Instantaneous Generation of Charge-Separated State on TiO_2 Surface Sensitized with Plasmonic Nanoparticles. *J. Am. Chem. Soc.* **2014**, *136*, 4343−4354.
(39) Townsend, E.; Bryant, G. W. Plasmonic Properties of Metallic Nanoparticles: The Effects of Size Quantization. *Nano Lett.* **2012**, *12*, 429−434.
(40) Ma, J.; Wang, Z.; Wang, L. W. Interplay between Plasmon and Single-Particle Excitations in a Metal Nanocluster. *Nat. Commun.* **2015**, *6*, 10107.
(41) Misawa, M.; Ryuo, E.; Yoshida, K.; Kalia, R. K.; Nakano, A.; Nishiyama, N.; Shimojo, F.; Vashishta, P.; Wakai, F. Picosecond Amorphization of SiO_2 Stishovite under Tension. *Sci. Adv.* **2017**, *3*, e1602339.
(42) Sigle, D. O.; Zhang, L.; Ithurria, S.; Dubertret, B.; Baumberg, J. J. Ultrathin CdSe in Plasmonic Nanogaps for Enhanced Photocatalytic Water Splitting. *J. Phys. Chem. Lett.* **2015**, *6*, 1099−1103.

DOI: 10.1021/acs.jpclett.7b02957
J. Phys. Chem. Lett. 2018, 9, 63−69